

# A Multilayer PCB Material Modeling Approach Based on Laminate Theory

Sven Rzepka<sup>1)</sup>, Frank Krämer<sup>1)</sup>, Oliver Grassmé<sup>1)</sup>, Jens Lienig<sup>2)</sup>

<sup>1)</sup> Qimonda Dresden GmbH & Co. OHG, Dresden, Germany

<sup>2)</sup> Dresden University of Technology, Institute of Electromechanical and Electronic Design, Germany  
Sven.Rzepka@Qimonda.com

## Abstract

After surveying the laminate theory, this paper presents a field proven 3-steps concept for modeling printed circuit boards (PCB). First, the behavior of the single plies is studied by means of a 3-D detailed model representing a typical cell. Afterwards, the laminate theory is applied to transfer the material data determined in the first step to a 3-layers model, which eventually allows modeling full PCBs in regular FEM simulations of complete electronic modules. Finally, the model of a 10-layer PCB is assembled and correlated to experimental data within the temperature range from 25°C to 150°C. Numerous experimental tests validate throughout the study that the model build-up this way is able to capture reality within a 5% accuracy band.

## Introduction

In electronic packaging, the simulation of mechanical and temperature cycling tests is a typical task of virtual prototyping. Its major goal is to assess the risk of interconnect failures in the solder joints between PCB and component induced by these loads. However, the accuracy of these assessments does not only depend on the solder material model but also on that of the PCB. Therefore, a target of 5% has been set as maximum difference between measurement and simulation results in validation studies of the PCB models.

Currently, fully isotropic or globally orthotropic approaches are widely used in modeling PCBs. Looking at the cross section of a single ply (Fig. 1), it already becomes evident that these approaches

may often not be sufficient to meet the 5% accuracy criterion. The complex mechanical behavior of a full PCB, which typically consists of five to nine plies and  $n+1$  electrical layers in addition, mostly requires adequate models to account for the laminate structure of this stack.

This paper presents a field proven 3-steps concept based on the laminate theory [3]. After surveying this theory, the behavior of the single plies is studied by means of a 3-D detailed model [2]. Afterwards, the laminate theory is applied to model these plies in an efficient way. Finally, the model of a 10-layer PCB is assembled and correlated to experimental data within a wide range of temperature. Numerous validation results show that the 5% accuracy criterion is met throughout the study.

## The Laminate Theory

The thickness of a PCB is very small as compared to its width and lengths. Hence, it could be described by 2-D models like membranes or plates. In addition, however, a PCB is composed of a soft matrix material, usually epoxy resin, reinforced by layers of glass fibers. This makes it a typical representative of the laminate materials also showing their characteristic anisotropic behavior. The stiffness parallel to the fibers is much larger than perpendicular to them. In addition, laminate films are much stiffer in tensile mode than in bending mode because the reinforcing fibers are not distributed uniformly across the film thickness but concentrated in the middle of each ply. In reality like a free drop event, bending and tension always occurs simultaneously. Likewise, realistic models must be able to capture both effects at the same time.

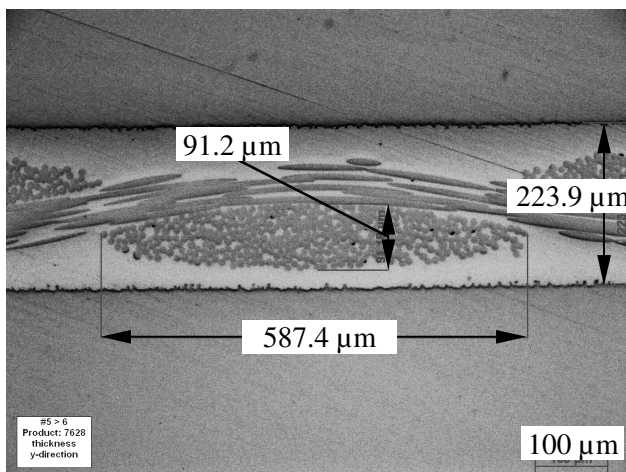


Figure 1: Cross section of a single ply of type 7628 and the measurements of a fiber bundle in Y direction.

The laminate theory [3] exactly accounts for this. It was developed based on Timoshenko general plate theory and combines the membrane and the plate states. The membrane loads are only acting in-plane causing tensile or shear deformations. Here, stresses are related to strains. The plate loads are acting perpendicular to a plane causing bending. In this case, moments are related to curvatures.

In the perfectly symmetric case, i.e., when the plies above the center plane are mirror-identical to those of the lower half of the stack, the membrane and plate states are independent of each other. Otherwise, they are coupled. Physically, this causes the laminate to bend even when hanging a weight on it actually causing a perfect tensile load. The softer side of the laminate would still extend more than the stiffer side. Mathematically, couple terms are needed to account for this effect.

Being an analytical method, the laminate theory is based on some assumptions more. The most important ones are:

1. Each layer has a uniform thickness and homogeneous or quasi-homogeneous material properties.
2. The material behavior of each layer is linear elastic in both modes, tension and bending.
3. The thickness of the laminate stays constant during the deformation and the deformations is small compared to the thickness. As consequence, the normal deformation in  $Z$  direction and the shear deformation  $YZ$  and  $XZ$  vanish.

With these assumptions, the general Hooke's law is reduced to two dimensions so that all three stiffness matrixes (membran, plate, coupling) just contain 3x3 elements: two in-plane tensile components and one shear component.

On the way to establishing the stiffness matrixes, the engineering constants of each individual layer are transformed into so-called reduced stiffness coefficient [4]. Finally, the 3x3 stiffness matrixes are filled with these coefficients.

Each ply  $k$  is orthotropic so that the material matrix is symmetric. In addition, there is no interaction between normal and shear coefficients. Therefore, the matrixes have only four non-zero independent coefficients as defined by eq. 1.

Now, the reduced stiffness coefficients of the matrix  $Q_k$  are known for every single layer with respect to its local coordinate system, in which  $x$  and  $y$  are the orthogonal axis. However, the orientation of

$$\begin{aligned} Q_{11_k} &= \frac{E_{x_k}}{1 - \nu_{xy_k} \cdot \nu_{yx_k}} \\ Q_{12_k} &= \frac{\nu_{yx_k} \cdot E_{x_k}}{1 - \nu_{xy_k} \cdot \nu_{yx_k}} = Q_{21_k} \\ Q_{22_k} &= \frac{E_{y_k}}{1 - \nu_{xy_k} \cdot \nu_{yx_k}} \\ Q_{33_k} &= G_{xy_k} \\ Q_{31_k} &= Q_{13_k} = Q_{32_k} = Q_{23_k} = 0 \end{aligned} \quad (1)$$

all layers must refer to a common global coordinate system before the overall behavior of a laminate can be calculated (Fig. 2). The alignment required is done by a transformation matrix  $T_k$ , which converts the set of material properties based on the local  $x-y$  coordinate system  $Q_k$  into those  $\bar{Q}_k$  based on the global  $X-Y$  system, eq. 2.

$$\bar{Q}_k = T_k \cdot Q_k \cdot T_k^T \quad (2)$$

This matrix of the reduced stiffness of layer  $k$  in global coordinates allows calculating the membrane and the plate stiffness matrixes,  $A_k$  and  $D_k$ , respectively, as seen in equation 3 and 4.

$$A_k = \bar{Q}_k \cdot h_k \quad (3)$$

$$D_k = \bar{Q}_k \cdot \frac{h_k^3}{12} \quad (4)$$

The coupling matrix  $B_k$  is a direct combination of the terms leading to equations 3 and 4. It constitutes the actual expansion of the general plate theory into the laminate theory.

$$B_k = \bar{Q}_k \cdot \frac{h_k^2}{4} \quad (5)$$

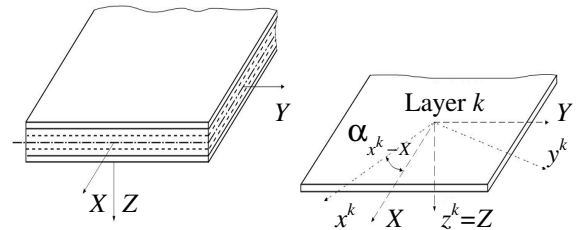


Figure 2: Single layer  $k$  with the coordinate system  $(x y z)^k$  rotated by an angle  $\alpha$  to the laminate with the global axes  $(X Y Z)$ .

Since the material properties are assumed constant across each layer's thickness  $h_k$ , the integral across the  $N$  layers of the laminate stack turns into a sum. Thus, the elements  $A_{ij}$ ,  $B_{ij}$ , and  $D_{ij}$  (with  $i, j = 1..3$ ) of the full laminate's stiffness matrixes can be calculated as follows:

$$\begin{aligned} A_{ij} &= \sum_{k=1}^N \bar{Q}_{ij_k} (z_k - z_{k-1}) \\ B_{ij} &= \frac{1}{2} \sum_{k=1}^N \bar{Q}_{ij_k} (z_k^2 - z_{k-1}^2) \\ D_{ij} &= \frac{1}{3} \sum_{k=1}^N \bar{Q}_{ij_k} (z_k^3 - z_{k-1}^3) \end{aligned} \quad (6)$$

where each layer stretches between  $z_{k-1}$  and  $z_k$ . The heights  $z_k$  are related to the neutral plane of the laminate stack. This results in positive and negative values. Therefore, the elements of the couple stiffness matrix vanish for symmetric laminate stacks so that the membrane and plate properties are then independent of each other. Usually, this case is approached by the real PCB stacks.

Finally, effective material properties of the full laminate stack can be derived by inverting the membrane stiffness matrix  $A$  and the plate stiffness matrix  $D$ , respectively, which results in the compliance matrixes  $a$  and  $d$ . This can be done easily if the coupling matrix is vanished due to symmetry within the stack. Then, the most important laminate properties can be calculated as follows:

$$\begin{aligned} E_x &= \frac{1}{a_{11}h} \\ E_y &= \frac{1}{a_{22}h} \\ F_x &= \frac{12}{d_{11}h^3} \\ F_y &= \frac{12}{d_{22}h^3} \end{aligned} \quad (7)$$

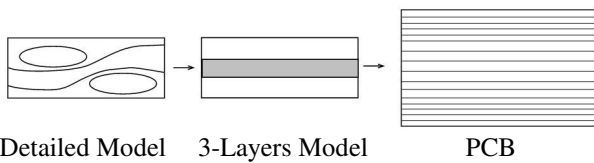


Figure 3: 3-step PCB modeling approach

The tensile stiffness  $E_x$  and  $E_y$  of the laminate (to be seen as effective Young's modulus along  $X$  and  $Y$ , respectively) as well as the bending stiffness  $F_x$  and  $F_y$  (effective flexural modulus) will subsequently be used to check the simulation results against the analytic model. The match should always be very close as long as the assumptions of laminate theory listed at the beginning of this section are applicable.

### FEM Modeling Approach

Although the PCB itself may be modeled quite precisely by a 2-D analytic approach, 3-D FEM models are usually required to capture the behavior of electronic modules under reliability test conditions adequately. To be consistent, a 3-D FEM representation of the PCB is needed as well. Hence, the goal of this paper is to present a 3-steps method, by which accurate PCB FEM models can be established efficiently based on the laminate theory.

Figure 3 depicts the three modeling steps. First, a detailed model is created. It covers a representative cell of a single ply. The data of the materials involved, i.e., the glass fiber bundles and the epoxy resin, is obtained from measurements and validated by simulating these measurement tests. The simulation results for the full cell are also validated by comparing to real tensile and bending experiments each performed on single ply samples along both fiber directions. Afterwards, the detailed model is used to determine all nine orthotropic material constants by simulating basic tensile and shear tests avoiding further real tests.

In the second step, the material properties provided by the detailed model are transferred to a 3-layers model, which eventually allows modeling full PCBs as needed in the simulations of electronic modules. In this model, the effect of the reinforcing glass fiber fabric is captured by the middle layer of each single ply while the outer layers of this ply consider isotropic resin only. After some calibration, each 3-layer stack is able to model the anisotropic behavior of the corresponding ply.

Finally, the model of the full PCB stack is created by piling up the three layer models accordingly supplemented by the conductive metal layers in between.

If the PCB consists of different ply types the steps one and two have to be executed repeatedly. Still, this 3-step toolbox approach proposed here is seen as the most efficient method of setting up pre-

cise PCB models. Creating and validating 3-layers models of the six different ply types and assembling them to full PCB models requires much less effort than measuring the complex properties of all the 70 PCBs currently being in use at Qimonda composed out of these six ply types.

### The Detailed Model

The material of the reinforcing fibers is E glass in all plies and the weaving technique is always the same as well (simple, denim like fabric). However, the number of fibers per bundle and the pitch of the bundles are specific to the ply type coded by a four-digit number, e.g., 1080, 2116, or 7628. Some ply types also show substantial differences between  $X$  and  $Y$  direction (e.g., ply 7628). Even when focusing on one ply type, differences are possible as the resin material and the total thickness of the ply can be varied meaning the resin content can be changed to adjust the final stiffness of the particular ply to specific requirements.

The detailed FEM model covers two pitches of the fiber reinforcement in both directions ( $X$  and  $Y$ ). The fiber bundles themselves are unidirectional reinforced mixtures of glass and epoxy. However, they are not perfectly straight but wavy (fig. 4a). Aligning the local element coordinate systems accordingly still allows accounting for the high stiffness along the axis of the fiber bundle and the lower stiffness normal to it easily. The transformation of the material properties into the global coordinate system is later on performed by the FEM code automatically. The complete model consisting of the fiber fabric and the resin is shown in figure 4b.

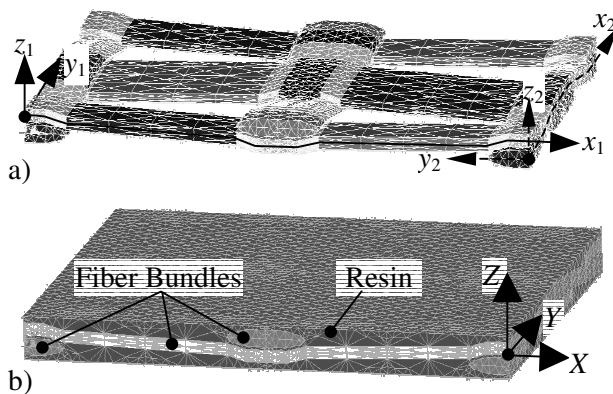


Figure 4: Detailed FEM model (ply type 7628)  
a) Glass fiber fabric with its element coordinate system, b) Complete model with the global coordinate system

Because of their arbitrariness in orientation and shape, the fiber bundles as well as the volume of pure resin in between are meshed with tetrahedral elements. Considering parameters for all input details, this model is flexible to represent any single ply by a typical cell.

The material data of the fibers' E glass such as Young's modulus  $E_{Glass}$  is very stable across the typical temperature range electronic modules operate. In addition, it is well documented [1]. The temperature dependent Young's modulus  $E_{Epoxy}$  of the resin type ITEQ-IT150 was measured.

The fiber bundles consist of a mixture of glass fibers and epoxy. Knowing the Young's modulus of both constituencies, the glass volume content  $v_{Glass}$  can be extracted from tensile tests, which measure the effective Young's modulus of the fiber bundles  $E_{Bundle}$  along the fiber axis, by applying the rule of mixture [3] and [4], equation 8.

$$E_{Bundle} = v_{Glass} E_{Glass} + (1 - v_{Glass}) E_{Epoxy} \quad (8)$$

No reinforcement effect occurs in the directions perpendicular to the fiber axis. Here, the bundles behave like epoxy.

As example, samples of single plies are tested. A glass volume fraction of  $v_{Glass} = 70\%$  was determined for the ply type 1080 based on the tensile test results. Afterwards, a three point bending test was simulated based on this model. As shown in table 1, the simulation results match the measured values quite closely. Then, a 132  $\mu\text{m}$  thick ply of type 2116 was chosen as second example. Here, the glass volume fraction in the fiber bundles calibrated by tensile test results was fixed to 66%. Without further changes, the detailed model was again able to match the bending measurement results very well,

Table 1: Stiffness of ply type 1080 (Simulation is based on the detailed FEM model assuming 70% glass volume fraction in the fiber bundles)

	Tensile stiffness $E_x$ in [GPa]	Bending stiffness $F_x$ in [GPa]
Measurement ( $M$ )	12.0	5.1
Simulation ( $DM$ )	11.8	5.3
Relative Error ( $DM - M$ ) / $M$	-1.7%	3.9%

Table 2: Stiffness of a 132  $\mu\text{m}$  thick ply, type 2116 (Simulation assumes 66% glass in the fiber bundles)

	Tensile stiffness $E_X$ in [GPa]	Bending stiffness $F_X$ in [GPa]
Measurement ( $M$ )	14.8	6.1
Simulation ( $DM$ )	14.9	6.3
Relative Error ( $DM - M$ ) / $M$	0.7%	3.3%

table 2, although the magnitude was quite different with respect to both, the other ply type  $F_X(1080)$  and the tensile stiffness  $E_X(2116)$ . Therefore, the modeling approach seems to be valid and accurate.

Applying the calibrated and validated models, the nine independent parameters characterizing the plies' orthotropic material properties are determined by simulating basic shear and tensile tests. Of course, the accuracy of the data generated this way directly depends on the accuracy of the input parameters. In case of Young's modulus, the parameters have just been validated. The Poisson ratio of the epoxy was set to 0.27 in the range below glass transition temperature based on the wide spread data found in literature [5], [6]. Applying eq. 8 with the Young's moduli replaced by the Poisson's ratios,  $\nu_{xy}$  and  $\nu_{xz}$ , i.e., the effective Poisson's ratio of the fiber bundle in the direction influenced by the reinforcement along  $x$ , are calculated out of the Poisson ratio of the E glass (0.20) [1] and epoxy. The remaining Poisson ratio  $\nu_{yz}$  is equal to the value of pure epoxy since the glass fibers have no influence here. The shear modulus of the fiber bundle is then calculated by applying the rule of mixture accordingly, eq. 9, with  $G_{Glass}$  and  $G_{Epoxy}$  denoting the shear moduli of E glass and epoxy resin, respectively.

$$G_{XY} = \frac{G_{Epoxy} \cdot G_{Glass}}{(1 - \nu_{Glass})G_{Glass} + \nu_{Glass} \cdot G_{Epoxy}} \quad (9)$$

The modulus  $G_{XZ}$  has the same value like  $G_{XY}$  because the effect of the reinforcement is identical in both cases. However, the shear modulus of the remaining  $Y-Z$  plane is different.  $G_{YZ}$  is equal to  $G_{Epoxy}$ , the epoxy shear modulus, because the bundles are not reinforced along their width. Having defined all input parameters by now, the basic test can be simulated as listed in table 3 in order to

quantify the effective set of the nine material parameters for the complete ply layers. The results of these simulations are to be transferred to the 3-layers model afterwards. This is described in the next section.

### The 3-Layers Model

The detailed model allows explaining the differences in tensile and bending stiffness as effects of the composite structure of the single ply. It also allows determining the nine engineering constants of this orthotropic material. However, the detailed model cannot be applied to a full PCB. It would require way too many elements causing excessive computational efforts. Therefore, a model is now introduced, in which the thickness of the ply is split into just three layers, which may even be combined in a single finite element by means of the multilayer option of 3-D finite element like ANSYS element Solid46 or Solid186 [7]. This way, complete PCBs can be modeled as correctly and inexpensively as needed in industrial simulations of drop or thermal cycle tests of regular electronic modules.

The two outer layers of this model, i.e. the top and the bottom layers, represent the pure resin of the ply whereas the middle layer models the mixture of the glass fibers and the resin. The material models for the outer layers are readily available. The effective engineering constants for the middle layer need to be determined specifically for each ply type. This can also be done easily by applying the detailed model as described before. However, the thickness of the middle layer is the key parameter of this model approach requiring some further consideration.

The classical laminate theory considers plies with a uni-axial reinforcement by straight fibers [3].

Table 3: Summary of the necessary simulations for a complete data set of the orthotropic single plies

Test	Determined material properties
Tensile along $X$	$E_X, \nu_{XY}, \nu_{XZ}$
Tensile along $Y$	$E_Y, \nu_{YX}, \nu_{YZ}$
Tension along $Z$	$E_Z, \nu_{ZX}, \nu_{ZY}$
$Y-Z$ Shear	$G_{YZ}$
$X-Z$ Shear	$G_{XZ}$
$X-Y$ Shear	$G_{XY}$

In this case, the thickness of the middle layer may be set equal to that of the reinforcing fibers,  $t_{GLASS}$ . Consequently, a thickness of two fiber bundles might be assumed in the case of PCB plies, in which a woven glass fabric reinforces the laminate in two dimensions. At the first glance, this simple approach seems valid, as the real plies are always thicker than the fiber bundles at their crossings. However, simulation results prove this approach incorrect. Even after calibrating the resin-to-glass ratio in the middle layer along both fiber directions separately, the 3-layer model can still just match the tensile or the bending stiffness results computed by the detailed model but not both kinds of stiffness at the same time, table 4.

According to eq. (7), the tensile stiffness is inverse proportional to the height of the layer while the bending stiffness inversely depends on the layer height to the power of three. This means, both kinds of stiffness would qualitatively show the same change when the thickness of the middle layer is reduced but the reaction of the bending stiffness would be much larger in magnitude increasing the ratio between the two kinds of stiffness as needed to match the measurement results (tab. 4). Hence, the initial assumption of twice the height of the fiber bundles appears to be the upper limit while the actual effective thickness of the middle layer,  $h_{EFF}$ , must be lower. The lower limit is marked by the height of a single fiber bundle, as the middle layer is supposed to accommodate the reinforcement completely, i.e., the outer two layers shall model resin only.

Table 4: Computed stiffness of ply 2116 dependent on the thicknesses of the middle layer

	Tensile Stiffness in GPa		Bending Stiffness in GPa	
	$E_X$	$E_Y$	$F_X$	$F_Y$
Detailed Model ( $DM$ )	14.9	14.9	6.3	6.0
3-Layer Model ( $3L$ ) $h_{Middle} = 2 t_{GLASS}$	15.0	14.5	11.1	11.0
Relative Error ( $3L - DM$ ) / $DM$	0.7%	-2.7%	76%	82%
3-Layer Model ( $3L$ ) $h_{Middle} = h_{EFF}$	15.0	14.7	6.1	6.0
Relative Error ( $3L - DM$ ) / $DM$	0.7%	-1.3%	-3.2%	0%

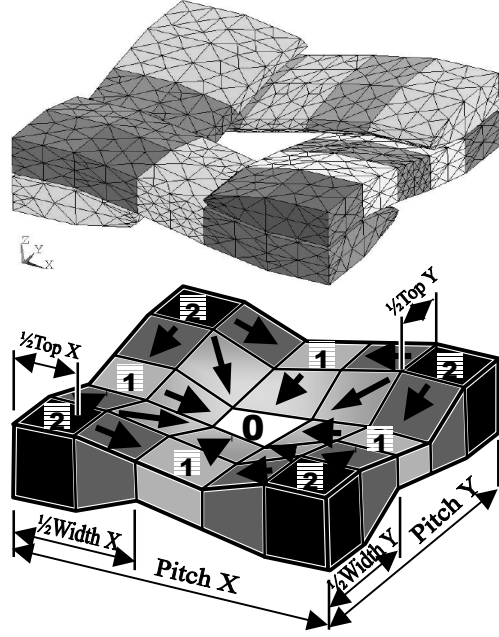


Figure 5: Model of the woven glass fiber bundles  
Top: Mesh of the detailed model,  
Bottom: Regions for determining the average height

Determining the effective thickness,  $h_{EFF}$ , the local height of the fiber bundles needs to be considered. Figure 5 shows the classes of heights by which the fabric of the glass fiber reinforcements can be modeled. Based on them, the average height is computed. Its value is specific to the ply type as it reflects the exact dimensions of the regions without glass fibers (0), with the full height of one (1) and two bundles (2), respectively, as well as of all the adaptive regions in between, which are interpolated linearly. The average height of the fiber bundles may differ between  $X$  and  $Y$  directions. Accordingly, the resin content follows inversely.

With the average fiber heights computed, the effective thickness of the middle layer,  $h_{EFF}$ , is determined by matching the measured values of both kinds of stiffness, tensile and bending, at the same time. In this optimization iteration, reducing  $h_{EFF}$  virtually shifts resin from the middle layer to the outer layers, which means an increase in effective stiffness of the middle layer (eq. 8), as the fiber dimensions do not change anymore and the overall volume of the 3-layer structure stays constant. The result of the optimization listed in lower rows of table 4 show all pairs of stiffness being within the 5% accuracy band. The small deviations remaining

are caused by measurement scatter, which affected the results of the detailed model, and the simplifications of linear interpolation when computing the average fiber heights. They are acceptable very well.

A real PCB usually consists of one particular type of resin only although several types are in use in general. Sometimes, even the type of glass fiber fabric is the same in all plies of the PCB so that each of them is labeled by the same four-digit number. Still, these plies do not have to behave all identically as their thickness and hence their over-all resin content may differ.

The 3-layers model introduced before is able to account for this variation in resin content easily. If in reality, the thickness of the individual ply is changed by adding or removing resin the thickness of the two outer layers needs to be adjusted in the model accordingly. The middle layer, which models all the anisotropic behavior, is not changed. Table 5 shows the validity of this concept as it lists the tensile stiffness of two plies both being of type 2116 but differing in different thickness by 17%. Right after typing in the correct thickness values, both models match the measurement results well within the 5% accuracy band. It really is worth noting that no further calibration was needed. This marks an advantage of the 3-layers model over the conventional approach, in which each ply of the laminate stack is modeled by one layer only. Thanks to the 3-layers approach, none of material models, i.e. neither that of the middle layer nor this of the resin, needed any adjustment although the resin content of the ply was raised substantially by increasing the ply thickness so that the ply stiffness was reduced accordingly. This flexibility of the 3-layers model concept is very beneficial to the industrial practice. DMA characterization sequences are needed only

Table 5: Tensile stiffness of 2 plies of type 2116, 132  $\mu\text{m}$  and 154  $\mu\text{m}$  thick, respectively

	Measurement	3-layers model	Deviation from measurement
<b>132 <math>\mu\text{m}</math> thick:</b> Tensile stiffness $E_X$ in [GPa]	14.8	15.0	1.4%
<b>154 <math>\mu\text{m}</math> thick:</b> Tensile stiffness $E_X$ in [GPa]	12.8	13.2	3.1%

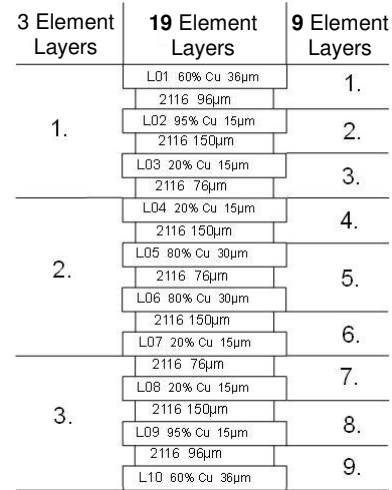


Figure 6: Stack-up of a PCB specimen with 10 copper layers and variants of FEM models

once per resin material and ply type while the additional variations in resin content are covered by a simple geometric assessment. Luckily, the modeling effort is also not increase when moving from the 1-layer to the 3-layers approach. The multi-layer elements provided by the commercial FEM codes usually allow accounting for 200 and more layers. This is more than needed.

### The PCB stack model

The scheme of one particular PCB stack-up is sketched in figure 6. It consists of 10 copper layers and 9 ply layers of type 2116 with different thicknesses.

In contrast to the plies, whose material behavior has already been modeled by now, the parameters of the copper layers are still to be determined. From the mechanical point of view, these layers may be seen as mixtures of copper and epoxy. The ratio between the two constituencies can be determined from the Gerber data specifically to each layer. Some of the signal layers contain less than 40% copper (e.g., layers 03, 04 and 07, 08 in fig. 6). In addition, the individual traces are so small that they do not reinforce this layer significantly. Hence, its behavior is clearly dominated by the epoxy. On the other hand, power and ground layers (such as layers 02 and 09) are often covered by more than 90% copper, which basically means full copper films just being pierced by some small holes, the so-called anti-pads around the vias. Consequently, these layers just behave like copper.

Besides these extreme cases, in which the film can be modeled as either resin or copper only, there is a range in which the model really needs to account for both constituencies. When the total amount of copper exceeds 40%, the film stiffness really is increased even with the individual traces all being very small and placed arbitrarily in the plane of the complete film. On the other hand, the traces are not able to control the film behavior completely as they are still just coupled by the soft matrix of epoxy resin material covering at least 10% of the layer's volume. Based on the assumptions indicated, i.e., many very small copper traces are distributed arbitrarily but homogeneously within the film, the resulting stiffness can be calculated according to the rule of mixtures as listed in equation 9 just with the shear modulus being replaced by the Young's modulus and the fiber content by that of the copper. Based on a Young's modulus of 127 GPa for copper and 2.5 GPa for epoxy, the resultant stiffness is computed as 6.1 GPa for the outermost layers L01 and L10 as they have a copper coverage of 60%. If the assumptions made are not valid at all locations the total PCB area may be split into regions.

In total, the model of the chosen PCB example consists of 10 effective copper layers and 9x 3 ply layers. Figure 6 shows three different options for capturing these 37 layers by multi-layer finite elements. In the most detailed approach, 19 element layers allow modeling each copper film and each ply by one separate element layer. Option 2 stretches each element across one copper film and its adjacent ply resulting in nine elements along the PCB thickness. Since the computation time scales roughly with the square of number of finite elements the models consists of, option 3 leads to the fastest simulations as it splits the PCB thickness into three elements only. However, increasing the complexity

Table 6: Measured and simulated bending stiffness of a 10 layers PCB

Measurement	Simulation Result based on models with		
	19 elements	9 elements	3 elements
18.8 GPa	19.1 GPa	19.4 GPa	19.7 GPa
Deviation from measurement	1.6 %	2.8 %	4.9 %

to be covered by one element reduces the accuracy of the numerical FEM result. In particular, models usually become stiffer when the mesh is coarsened. The results listed in table 6 clearly show this trend. The model of 19 element layers matched the measured stiffness most precisely while the 3-element-layers model shows the highest stiffness. Still, the accuracy of the 3-element-layers model is within the 5% tolerance range. Hence, this most efficient model is a valid option for practical applications.

### Temperature dependent material data

Electronic modules may be exposed to temperatures between  $-65^{\circ}\text{C}$  and  $150^{\circ}\text{C}$  during test and service and even to  $260^{\circ}\text{C}$  during manufacturing. Usually, the maximum temperature is above the glass transition region of the PCB resin  $T_G$  while the lower temperature is below it. Still, the PCB model must be valid within the full temperature range. Consequently, measurements and modeling need to cover this range applying all models and methods explained before.

Figure 7 shows the tensile stiffness of a  $154\ \mu\text{m}$  thick ply of type 2116 consisting of ITEQ-IT 150 resin as result of measurements and simulation within the temperature range between  $-25^{\circ}\text{C}$  and  $155^{\circ}\text{C}$ . It is worth noting that only the resin properties were calibrated during to the simulation while all geometric model parameters including the resin content ratio within the fiber bundles were kept at their values determined at room temperature. This way, the validity of the model approach was proven since the measured curve could be matched by simulation well within the 5% tolerance band indicated in the fig. 7 for most of the temperatures. Only at  $T_G$ , the deviation exceeds this limit reaching up to

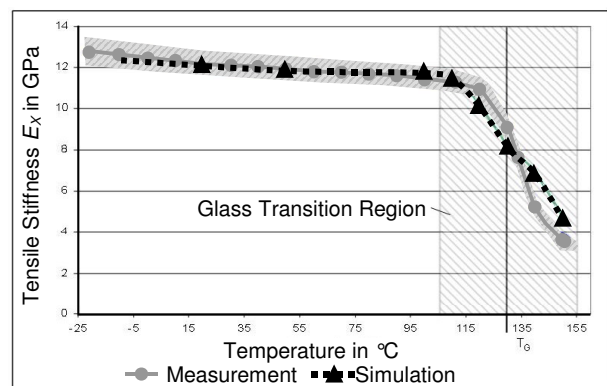


Figure 7: Temperature dependent tensile stiffness  $E_x$  of the  $154\ \mu\text{m}$  thick ply of type 2116

11%. However, experimental results also show increased scatter in this temperature range. Hence, the accuracy achieved is found sufficient.

With the material data of the single plies at hand, the PCB can be assembled. Of course, the temperature dependence of the resin within the copper layers must be taken into consideration. Below  $T_G$ , this is done by applying the rule of mixtures (eq. 9) as mentioned before. As seen in fig. 8, close match between the measured and modeled results of the full PCB bending stiffness can be achieved this way for all temperatures below  $T_G$ . However, the PCB model clearly is too stiff above  $T_G$  (see upper dotted line in fig. 8). In a second attempt, the PCB stack was modeled with all copper layers fully replaced by epoxy. This model is much too soft below the glass transition range. However, it matches the measured curve very well above the glass transition temperature. Obviously, the reinforcing effect of the copper layers disappears when the epoxy approaches the rubber state. Most likely, this is the result of the visco-elastic relaxation within the epoxy. This means, fully disregarding the reinforcing effect of the copper above  $T_G$  models the limiting case of complete relaxation within a very short time. Correspondingly, taking 100% of the reinforcing effect into account independent of any time below the glass transition range represents the other limiting case, which is being perfectly stable. As seen in figure 8, this simple approach to visco-elasticity has lead to valid modeling results at all temperatures except for the range of  $\pm 10$  K around  $T_G$ . Here, a linear interpolation between the two extreme cases was able to close the gap, which means 50% of the reinforcing effect determined at low temperature (e.g., at room temperature) had to be considered at  $T_G$ . Applying this approach, the modeled stiffness curve stayed within the 5% tolerance band across the full temperature range (fig. 8).

Of course, the specific parameters like the width of the intermediate range of temperature, which was  $\pm 10$  K in the current example, or the magnitude of  $T_G$  in general are all specific to the particular configuration within this PCB stack and also depend on the load conditions - furthestmost on the temperature time profile. Nevertheless, the PCB models created the way presented here may still be applicable quite broadly in industrial simulations as the conditions of interest often do not change so frequently. For example, the number of PCB resins used within one

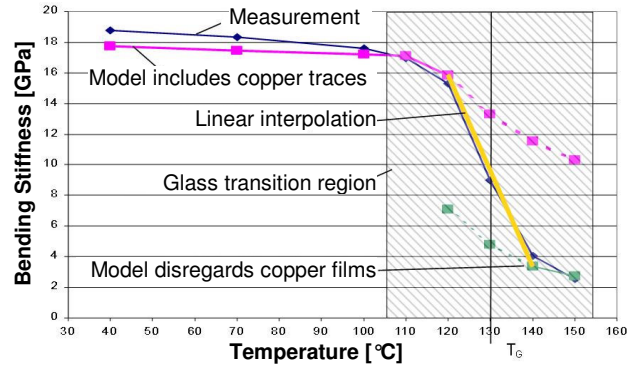


Figure 8: Measured and modeled temperature dependent bending stiffness of a full PCB

company is limited and often stays stable for some years. The soldering profile is also kept unchanged for quite some time. The temperature cycle test conditions even follow international standards with most of them having been in place for a few decades already.

Therefore, the concept for modeling PCBs is shown capable of providing accurate results well within a 5% tolerance band to measured data in an effective way not only at one temperature but across the full range relevant in electronics packaging. This gain in accuracy over existing models, which may not even be able to distinguish between bending and tensile stiffness, neither requires measurement efforts exceeding what is acceptable in industrial practice nor does it lead to excessive simulation run times.

## Conclusions

This paper has presented an industry proven methodology for creating accurate PCB models based on the laminate theory. The methodology consists of 3 steps. First, a representative cell of each ply type used within the PCB stack is investigated by a detailed 3-D FEM model. The cell covers at least one pitch of the woven fiber bundle fabric in both planar directions and the full thickness of the ply with all the epoxy resin. After the initial calibration of the material properties of the fiber bundles, which consist of epoxy being uni-axially reinforced by glass fibers, this model is ready to determine the parameters describing the effective orthotropic material behavior of the full ply. The validation of this calibration was done by comparing the tensile and the bending stiffness obtained by measurement and simulation.

Secondly, a 3-layers model is introduced, which allows the ply properties to be modeled by multi-layer elements. The middle layer accounts for the complete glass fiber grid of this ply while the top and the bottom layers just model isotropic resin. The effective thickness of the middle layer is calculated by averaging the fiber bundle geometry within this characteristic cell and by calibrating both kinds of stiffness, bending and tensile, to the corresponding measurement results simultaneously. The 3-layers approach offers an important flexibility with respect to the total thickness of the ply by which its resin content is adjusted in reality. Following the 3-layers approach, the simulation results spontaneously meet the accuracy target of maximum 5% deviation from measurement even when the ply thickness is changed by 17% without any further material parameter adjustment done. The variation in the ply behavior is completely covered by considering the respective resin thickness values.

In the third step, the complete PCB stack is compiled based on the 3-layers models of each ply type involved in this stack and the copper layers between the plies. Here, three qualitatively different cases have been identified with respect to the copper coverage. Below 40% copper content, the layers just behave like resin, while they behave like full of copper when the coverage is beyond 90%. When copper coverage is in between these levels, the effective stiffness is computed by the rule of mixtures except for the copper cannot be seen as very small traces arbitrarily yet homogeneously distributed within the film. In those configurations, the single PCB model needs to be split into a few each dedicated to one region, in which either one of the three cases fully applies.

Validated by a bending experiment, it has been shown that the 3-layers approach can be applied real to PCBs. Utilizing the multi-layer option, just three elements suffice along the PCB thickness although the example laminate consisted of 37 layers in total. The accuracy of this effective model clearly met the 5% requirement. Obviously, the limitation of the classical laminate theory, which is the neglect of bending moments, is not affecting this multi-layer approach.

Finally, this modeling methodology was extended to the full temperature range relevant to electronics packaging. It was found that the PCB model developed so far was able to replicate the behavior

seen in the bending experiments up to about 10 K below the glass transition temperature. Above this, the PCB was predicted too stiff, although the behavior of all individual plies matched very well with the measurements. A second PCB model, in which the copper films were all replaced by pure epoxy, was able to follow the real behavior at temperatures beyond about 10 K above  $T_G$ . Within the transition range of temperature, a linear interpolation between the limiting cases of no visco-elastic relaxation below the glass transition range and complete, fast relaxation above that range was done. It finally enabled the modeled stiffness curve of the full PCB stack to stay well within the 5% tolerance band around the measured values across all temperatures.

This way, the 3-steps concept of modeling PCB based on the laminate theory has been validated. Utilizing the multi-layer elements provided by the commercial FEM codes, the resulting 3-D models allow reliable simulation assessments of full electronic modules to be performed with very reasonable computational time.

## References

1. Data of E glass fiber, generic; MatWeb.com, Jan 20, 2008, <http://www.matweb.com/search/DataSheet.aspx?MatID=900>
2. Wielage/ Müller/ Lampke: Berechnung elastischer Eigenschaften gewebeverstärkter Verbundwerkstoffe. Werkstoffe in der Fertigung, Heft 1, 2005, pp. 23-5
3. Tsai/ Hahn: Introduction to composite materials, 1980. Lancaster: Technomic Publishing Company.
4. H. Altenbach/ J. Altenbach/ Naumenko: Ebene Flächentragwerke, 1998. Berlin/ Heidelberg: Springer Verlag
5. Schwarzl: Polymermechanik, 1990. Berlin/Heidelberg: Springer Verlag
6. Hellrich/ Harsch/ Haenle: Werkstoff-Führer Kunststoffe, 1975. München/Wien: Carl Hanser Verlag
7. Ansys Inc., Ansys Release 10.0 Documentation, 2005.